2012

Piezoelectric Wafer Active Sensors in Lamb Wave-Based Structural Health Monitoring

Lingyu Yu
University of South Carolina - Columbia, yu3@engr.sc.edu

Victor Giurgiutiu
University of South Carolina - Columbia, victorg@sc.edu

Publication Info

Published in *Journal of Materials*, Volume 64, Issue 7, 2012, pages 814-822.

Yu, L. & Giurgiutiu, V. (2012). Piezoelectric wafer active sensors in Lamb wave-based structural health monitoring. *Journal of Materials*, 64(7), 814-822.
http://dx.doi.org/10.1007/s11837-012-0362-9

JOM, Vol. 64, No. 7, 2012
DOI: 10.1007/s11837-012-0362-9

Piezoelectric Wafer Active Sensors in Lamb Wave-Based Structural Health Monitoring

LINGYU YU[1,3] and VICTOR GIURGIUTIU[2]

1.—University of South Carolina, 300 South Main Street, RM #A111, Columbia, SC 29208, USA.
2.—University of South Carolina, 300 South Main Street, RM #A222, Columbia, SC 29208, USA.
3.—e-mail: yu3@cec.sc.edu

Recent advancements in sensors and information technologies have resulted in new methods for structural health monitoring (SHM) of the performance and deterioration of structures. The enabling element is the piezoelectric wafer active sensor (PWAS). This paper presents an introduction to PWAS transducers and their applications in Lamb wave-based SHM. We begin by reviewing the fundamentals of piezoelectric intelligent materials. Then, the mechanism of using PWAS transducers as Lamb wave transmitters and receivers is presented. PWAS interact with the host structure through the shear-lag model. Lamb wave mode tuning can be achieved by judicious combination of PWAS dimensions, frequency value, and Lamb mode characteristics. Finally, use of PWAS Lamb wave SHM for damage detection on plate-like aluminum structures is addressed. Examples of using PWAS phased array scanning, quantitative crack detection with array imaging, and quantitative corrosion detection are given.

INTRODUCTION

Recent advancements in sensors and information technologies have resulted in new methods for structural health monitoring (SHM) of the performance and deterioration of structures. SHM refers to the procedure used to assess the condition of structures so that their performance can be monitored at any time and damage can be detected at an early stage, thus increasing the reliability, safety, and efficiency of the structures. The process of SHM typically involves monitoring of a structure over a long period of time using permanently installed sensors, data interpretation algorithms to extract damage-related information from the sensory measurements, and analysis of the damage extent in order to determine the current state of the structure.

Current ultrasonic inspection is a time-consuming operation that requires meticulous through-thickness C-scans over large areas. One method to increase the efficiency of plate-like structures is to utilize Lamb waves (i.e., guided waves in plate-like structures) instead of conventional pressure waves. One attractive feature of Lamb waves for SHM purpose is the creation of stresses across the entire thickness of the plate, allowing for the interior as well as the exterior structures to be interrogated. They also exhibit low attenuation over large distances, thereby allowing for large-area inspection with minimum usage of sensors.

SHM requires the development of small, lightweight, inexpensive, unobtrusive, minimally invasive sensors to be embedded in the structures at acceptable cost to perform on-demand structural interrogation without the need for disassembly. Such sensors should be able to scan the structure and identify the presence of defects and incipient damage. In recent years, piezoelectric wafer active sensors (PWAS) permanently attached to the structure have been used for Lamb wave generation and detection during the SHM process. The purpose of a PWAS transducer is to excite stress wave motion or convert this motion into an electrical signal. PWAS are piezoelectric sensors with elements made of piezoelectric materials. PWAS are no more expensive than conventional high-quality resistance strain gages. However, PWAS performance far exceeds that of conventional resistance strain gages, because they can be used as active interrogators. PWAS can be used in high-frequency applications at hundreds of kHz and beyond. Use of PWAS for Lamb wave SHM has been pursued by many researchers.[1–5]

(Published online July 10, 2012)

PIEZOELECTRIC INTELLIGENT MATERIALS

Piezoelectric materials are intelligent materials that couple the mechanical and electrical domains. In 1880, Jacques and Pierre Currie found that, when subject to a mechanical force, these materials become electrically polarized. The converse of this relationship also is true: they lengthen or shorten when exposed to an electric field. These behaviors are known as the *piezoelectric effect* and *inverse piezoelectric effect*, respectively, from the Greek word "piezein," meaning to press or squeeze.[6] Although these materials rarely contain iron, they are often called ferroelectric materials because their electrical behavior is analogous to the magnetic behavior of ferromagnetic materials. Piezoelectric materials have been adapted for an impressive diversity of sensing and actuation applications.

Piezoelectric Materials

For many years, natural crystals such as quartz and tourmaline were the exclusive source of piezoelectric capabilities, and many types of products were developed with these materials. In recent decades, however, and especially since the mid-1960s, manmade materials, piezoelectric ceramics prepared from metallic oxides, have replaced natural materials in many applications. Piezoelectric ceramics can be hundreds of times more sensitive to electrical or mechanical input than natural materials, and the composition, shape, and dimensions of the ceramic can be tailored to meet the requirements of a specific purpose.[6] Piezoelectric ceramics are physically strong, chemically inert, and immune to humidity or other atmospheric influences, and they can be manufactured relatively inexpensively. Piezoelectric ceramics have enabled designers to employ the piezoelectric effect and the inverse effect in many new applications.

To manufacture piezoelectric ceramics, fine powders of the component metal oxides are mixed in specific proportions, and then heated to form a uniform powder. The powder is mixed with an organic binder and pressed, calendered, or molded into desired shapes (disks, rods, plates, etc.).[6] The ceramic shapes are fired according to a specific time and temperature program, during which the powder particles sinter and the material attains a dense, crystalline structure. The shapes are then cooled and further shaped or trimmed. If needed, electrodes are applied to the appropriate surfaces.

Above the Curie point of the raw ceramic, each perovskite crystal in each grain exhibits a simple cubic symmetry with no dipole moment (Fig. 1a). However, below the Curie point, each crystal exhibits its tetragonal or rhombohedral symmetry and its structure carries a dipole moment (Fig. 1b). The dipole moments are oriented differently among different crystal grains; that is to say, although each grain carries a net dipole moment, the ceramic element exhibits no overall polarization since the dipole moments are randomly oriented in the crystal grains in the ceramic (Fig. 1a). To attain polarization in a raw ceramic, the material needs to be poled or polarized.

The polarization is achieved by exposing the ceramic to a strong direct-current (DC) electric field, usually at a high temperature, slightly above the Curie point. The combination of the electric field and heating produces motion of the electronic dipoles. The strong electric field makes the dipoles reorient along the direction of the electric field (Fig. 1b), while the heat allows the dipoles to rotate freely, since the material is softer at higher temperature. Then, the electric field is removed and the material is quickly cooled down. Most of the dipoles are locked into the aligned configuration, giving the ceramic a permanent polarization (Fig. 1c). Note that, during the polarization, the ceramic also undergoes elongation along the direction of the electric field and this deformation is retained after the removal of the electric field. The permanent deformation makes the ceramic anisotropic; i.e., its properties differ according to the direction in which they are measured.

Piezoelectric Principles

For linear piezoelectric materials, the interaction between the electrical and mechanical variables can

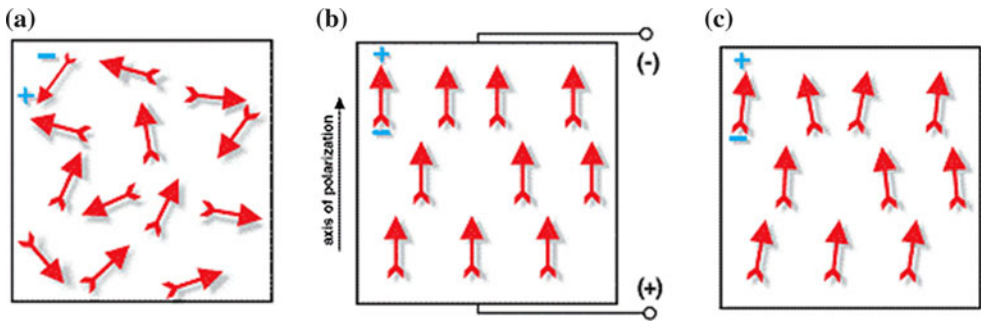

Fig. 1. Poling (polarization) of a piezoelectric ceramic: (a) raw piezoelectric ceramic, no overall polarization; (b) poling with applied external DC electric field and increased temperature; (c) after poling, the ceramic is polarized and anisotropic.[6]

be described by linear equations.* Linear constitutive equations between mechanical and electric variables, for direct and inverse piezoelectric effects, take the following tensorial form[7]:

$$\langle \text{Actuation} \rangle \quad S_{ij} = s^E_{ijkl} T_{kl} + d_{kij} E_k, \tag{1}$$

$$\langle \text{Sensing} \rangle \quad D_i = d_{ikl} T_{kl} + \varepsilon^T_{ik} E_k, \tag{2}$$

where S_{ij} and T_{ij} are the strain and stress (mechanical variables) and E_k and D_i are the electric field and electric displacement (electrical variables). s^E_{ijkl} is the mechanical compliance at zero electric field, and ε^T_{ik} are the dielectric constants at zero mechanical stress. d_{kij} and d_{ikl} signify the coupling between the electrical and mechanical variables, i.e., the charge per unit stress and the strain per unit electric field. Equation 1 is usually referred to as the actuation equation and Eq. 2 as the sensing equation. Usually the general three-dimensional (3D) constitutive equations can be simplified by considering symmetry associated with elastic, electrical, and electromechanical properties and written in *Voigt* notation.[8]

Since a piezoelectric ceramic is anisotropic, the physical constants relate to both the direction of the applied mechanical or electrical variables and to the directions perpendicular to the applied variables. Consequently, each constant generally has two subscripts that refer to the directions of the two related quantities, as for stress and strain in elasticity. The direction of positive polarization is usually aligned with direction 3 (or the Z-axis) of a rectangular system. Shear directions are represented by the subscripts "4," "5," and "6." Some important and frequently used piezoelectric constants can be found in detail in Ref. [6].

Common Operating Modes

The convention with piezoelectric materials is to align direction 3 with the polarization of the material; thus, directions 2 and 3 are in the plane of the transducer. Usually the ceramic is made in wafer shape, i.e., with the plane dimensions being much larger than the thickness.

Thickness Mode (d_{33} Mode)

In the thickness mode, the d_{33} coupling effect is used (Fig. 2). Conventionally, it is assumed that only the stress and electric field along direction 3 are nonzero ($T_3, E_3 \neq 0$) and that only the strain and electric displacement in direction 3 are of interest; i.e., the constitutive equations of the d_{33} mode are

$$S_3 = s^E_3 T_3 + d_{33} E_3, \tag{3}$$

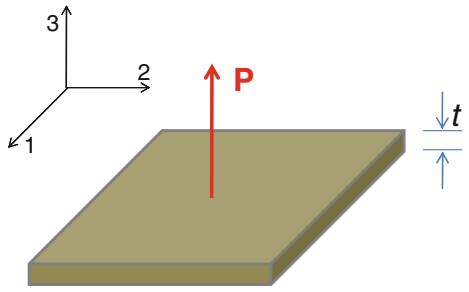

Fig. 2. Thickness mode.

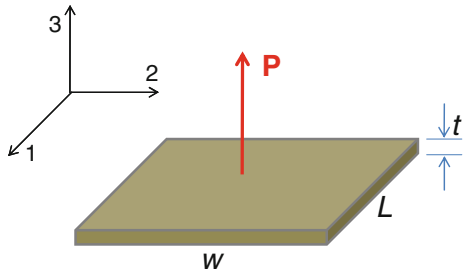

Fig. 3. In-plane mode.

$$D_3 = d_{33} T_3 + \varepsilon^T_{33} E_3. \tag{4}$$

The piezoelectric coupling d_{33} is used in this mode. These relations can be expressed in terms of the force (F), displacement (u_3), voltage (V), and charge (q) as well. Assuming uniform strain S_3, uniform stress T_3, and uniform electric field E_3, and using the relation between electric displacement D_3 and charge q ($q = D_3 A$, where A is the ceramic area), we have

$$u_3 = s^E_3 \frac{tF}{A} + d_{33} V, \tag{5}$$

$$q = d_{33} F + C_0 V, \tag{6}$$

with $C_0 = \varepsilon^T_{33} A/t$ being the wafer's capacitance. The resulting current can be obtained by integrating the charge q over time. Conventional ultrasonic transducers usually operate in d_{33} mode.

In-Plane Mode (d_{31} Mode)

In the in-plane mode, the d_{31} coupling effect is used (Fig. 3). Conventionally, it is assumed that only stress along direction 1 and electric field along direction 3 are nonzero ($T_1, E_3 \neq 0$) and only strain in direction 1 and electric displacement in direction 3 are of interest; i.e., the constitutive equations of the d_{31} mode are

$$S_1 = s^E_1 T_1 + d_{13} E_3, \tag{7}$$

$$D_3 = d_{31} T_1 + \varepsilon^T_{33} E_3. \tag{8}$$

*ANSI/IEEE standard 176-1987 on piezoelectricity.

The piezoelectric coupling d_{31} is used in this mode. These relations can be expressed in terms of force (F), displacement (u_1), voltage (V), and charge (q) as well. Assuming uniform strain S_1, uniform stress T_1, and uniform electric field E_3, and using the relation between electric displacement D_3 and charge q ($q = D_3A$, where A is the ceramic area), we have

$$u_1 = s_3^E \frac{LF}{\mathrm{wt}} + \frac{d_{13}L}{t}V, \tag{9}$$

$$q = \frac{d_{31}L}{t}F + \frac{\varepsilon_{33}^T wL}{t}V. \tag{10}$$

The resulting current can be obtained by integrating the charge q over time. Piezoelectric wafer-type transducers usually operate in d_{31} mode at low frequency and in d_{33} mode at very high frequency (above MHz).

PIEZOELECTRIC WAFER ACTIVE SENSORS AND LAMB WAVE SHM

For SHM applications, one way of using PWAS is as embedded ultrasonic transducers, acting as both Lamb wave exciters and detectors. PWAS couple their in-plane motion with the particle motion of Lamb waves on the material surface. The in-plane PWAS motion is excited by the applied oscillatory voltage through the d_{31} piezoelectric coupling. The PWAS ultrasonic transducer operation is fundamentally different from that of conventional ultrasonic probes:

(1) PWAS achieve Lamb wave excitation and sensing through surface "pinching" (in-plane strains), while conventional ultrasonic probes excite through surface "tapping" (normal stress);
(2) PWAS are strongly coupled with the structure and follow the structural dynamics, while conventional ultrasonic probes are relatively free from the structure and follow their own dynamics;
(3) PWAS are nonresonant, wideband devices, while conventional ultrasonic probes are narrow-band resonators.

As active sensors, PWAS interact directly with the structure and find its state of health and reliability through the use of ultrasonic Lamb waves. Similar to conventional ultrasonic transducers, PWAS can operate in pitch-catch, pulse-echo, or be wired into a phased array to implement structural scanning.

PWAS Lamb Wave Excitation and Reception

Lamb waves can exist in two basic types: symmetric (designated as S0, S1, etc.) and antisymmetric (designated as A0, A1, etc.). For each propagation type, a number of modes exist, corresponding to solutions of the Rayleigh–Lamb equation.[9] Lamb waves are highly dispersive, and their speed depends on the product of the frequency and the plate thickness. Details of Lamb wave theory can be found in many references.[9–12]

The excitation of Lamb waves by PWAS is studied by considering the excitation applied by the PWAS through a surface stress $\tau = \tau_0(x)e^{j\omega t}$ applied to the upper surface of a plate in the form of shear-lag adhesion stresses over the interval $(-a, +a)$. Applying a space-domain Fourier-transform analysis of the basic Lamb wave equations yields the strain wave and displacement wave solutions as[13]

$$\varepsilon_x(x,t)|_{y=d} = -i\frac{a\tau_0}{\mu}\left[\sum_{\xi^{\mathrm{S}}}\sin(\xi^{\mathrm{S}}a)\frac{N_{\mathrm{S}}(\xi^{\mathrm{S}})}{D'_{\mathrm{S}}(\xi^{\mathrm{S}})}e^{i(\xi^{\mathrm{S}}x-\omega t)} + \sum_{\xi^{\mathrm{A}}}\sin(\xi^{\mathrm{A}}a)\frac{N_{\mathrm{A}}(\xi^{\mathrm{A}})}{D'_{\mathrm{A}}(\xi^{\mathrm{A}})}e^{i(\xi^{\mathrm{A}}x-\omega t)}\right], \tag{11}$$

$$N_{\mathrm{S}} = \xi\beta\left(\xi^2+\beta^2\right)\cos(\alpha d)\cos(\beta d),$$
$$D_{\mathrm{S}} = \left(\xi^2-\beta^2\right)^2\cos(\alpha d)\sin(\beta d) + 4\xi^2\alpha\beta\sin(\alpha d)\cos(\beta d),$$
$$N_{\mathrm{A}} = \xi\beta\left(\xi^2+\beta^2\right)\sin(\alpha d)\sin(\beta d),$$
$$D_{\mathrm{A}} = \left(\xi^2-\beta^2\right)^2\sin(\alpha d)\cos(\beta d) + 4\xi^2\alpha\beta\cos(\alpha d)\sin(\beta d),$$

where ξ^{S} and ξ^{A} are the zeros of D_{S} and D_{A}, respectively. We can note that these are the solutions of the Rayleigh–Lamb equation. Raghavan and Cesnik[14] extended these results to the case of a circular transducer coupled with circular-crested Lamb waves and proposed the following corresponding tuning prediction formulae based on Bessel functions:

$$\varepsilon_r(r,t)|_{z=d} = \pi\frac{\tau_0 a}{\mu}e^{i\omega t}\left[\sum_{\xi^{\mathrm{S}}}J_1(\xi^{\mathrm{S}}a)\xi^{\mathrm{S}}\frac{N_{\mathrm{S}}(\xi^{\mathrm{S}})}{D'_{\mathrm{S}}(\xi^{\mathrm{S}})}H_1^{(2)}\left(\xi^{\mathrm{S}}r\right) + \sum_{\xi_{\mathrm{A}}}J_1(\xi^{\mathrm{A}}a)\xi^{\mathrm{A}}\frac{N_{\mathrm{A}}(\xi^{\mathrm{A}})}{D'_{\mathrm{A}}(\xi^{\mathrm{A}})}H_1^{(2)}\left(\xi^{\mathrm{A}}r\right)\right]. \tag{12}$$

An important characteristic of PWAS, which distinguishes them from conventional ultrasonic transducers, is their capability of tuning into various Lamb wave modes. A comprehensive study of these prediction formulae in comparison with experimental results has recently been performed by Giurgiutiu.[13] Equation 11 contains a $\sin(\xi a)$ behavior that displays maxima when the PWAS length $l_a = 2a$ equals an odd multiple of the half-wavelength, and minima when it equals an even multiple of the half-wavelength. A complex pattern of such maxima and minima emerges, since several Lamb modes, each with its own different wavelength, coexist at the same time. An example is given here. On a 1-mm-thick aluminum plate installed with 7-mm round PWAS, within an operation frequency range of 0–500 kHz,

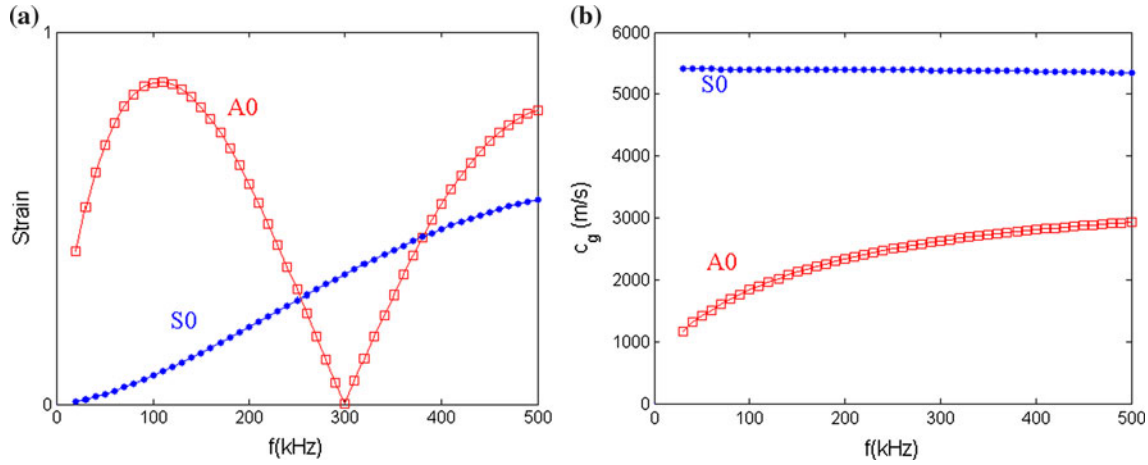

Fig. 4. Frequency tuning for PWAS on a 1-mm aluminum plate: (a) strain response at various frequencies for each Lamb mode; (b) group velocity at various frequencies.

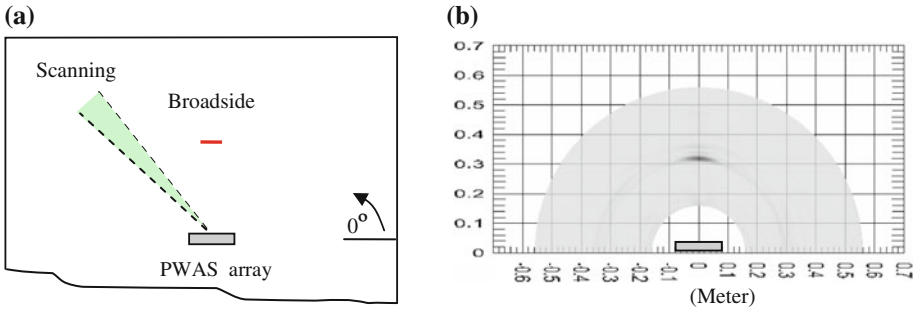

Fig. 5. PWAS phased array imaging on 1-mm aluminum plate with a 20-mm broadside crack: (a) specimen layout; (b) scanning image of the upper side of the plate.

two Lamb wave modes (A0 and S0) exist simultaneously (Fig. 4). However, as shown in the strain plot (Fig. 4a), there are frequency values where one of the two modes is nearly suppressed. At 300 kHz, the A0 mode vibration is very small, leaving the S0 mode to dominate. Group velocity versus frequency plots of the S0 and A0 modes are shown in Fig. 4b. We can see that, within the 0–500 kHz range, the S0 mode velocity is almost constant; i.e., the S0 mode is much less dispersive compared with the A0 mode.

PWAS Lamb Wave SHM

Phased Array Scanning

PWAS can also be wired as phased arrays to detect damage in thin-wall structures. The PWAS phased array application allows large structural areas to be monitored from a single location. The phased array application utilizes beam steering concepts, differentially firing various elements of the phased array such that constructive/destructive interference of all the transducers forms a wave beam in a certain direction.[13] Our previous work showed that the minimum detectable size on a 1-mm aluminum plate using a linear eight-PWAS (7 mm diameter) phased array is 1.57 mm.

An example of using a linear eight-PWAS phased array to detect and locate a 20-mm simulated crack on a 1-mm aluminum plate is given in Fig. 5a. The phased array was installed in the middle of the plate and used to scan the upper side from 0° to 180°. In the array, sensors were put side by side with a 1-mm gap. During interrogation, each PWAS in turn serves as the actuator sending out a three-count tone-burst signal, while others are used as sensors to receive the structural responses in a round-robin pattern. After the data are collected, they are postprocessed by the embedded ultrasonic structural radar (EUSR) algorithm to generate a virtual beam and the scanning two-dimensional (2D) image.[15] The result is shown in Fig. 5b. A highlighted shade about 305 mm in front of the array at 90° clearly indicates the presence of the broadside crack in the plate. However, to measure the size of the crack, additional image processing needs to be developed.

Crack Detection with Focusing Array Imaging

Unlike phased arrays, where sensors are physically close to each other, arrays consisting of a network of spatially distributed PWAS transducers

can also be used to inspect an area inside or outside the network. In the network, one PWAS sends out an interrogating guided wave. When the wave encounters damage, the wave is scattered. By differentiating the pristine and damaged signals, a scatter signal can be obtained. One advantage of using scatter signals is that this minimizes the influence caused by boundaries or other structural feature, which otherwise complicate the Lamb wave analysis.

The construction of the sparse array is based on a synthetic time-reversal concept presented by Wang et al.[16] The assumptions are (1) the wave scattering is solely caused by the defect in the structure, and (2) the detection is performed with a nondispersive single Lamb mode. The defect shows up as a wave packet in the scatter signal, and its arrival time depends on the total distance from transmitter T_i at (x_i, y_i) to the scatterer, and from the scatterer to the receiver R_j at (x_j, y_j). If we shift the wave packet by the traveling time, it will be completely back-propagated to the time origin of its actuation. To determine the pixel value at a random location $Z(x, y)$ in the structural plane, a group of measurements from the sensing array are needed. The back-propagation time and the data fusion algorithm for the array imaging are

$$\tau_Z = \frac{\sqrt{(x_i - x)^2 + (y_i - y)^2} + \sqrt{(x - x_j)^2 + (y - y_j)^2}}{c_g}, \tag{13}$$

$$P_Z(t_0) = \prod_{i=1}^{M} \prod_{j=1}^{M} s_{ij}(\tau_Z), \quad i \neq j. \tag{14}$$

Detection of a 23-mm crack at (315, 249) was performed on a 1-mm-thick 2024-T3 aluminum plate. A total of seven PWAS were installed randomly at locations indicated in Fig. 6 on the left. The Lamb wave mode used here is the S0 mode at 310 kHz. The first detection was conducted by PWAS 0, 2, 3, and 6 with the crack inside the sensor array (Fig. 6a). The resulting image is shown in Fig. 6b. It is seen that the two tips of the crack form two strong scatterers of the Lamb wave and generated two strong, intensified spots on the images. From the estimations of the crack tip locations at (309, 255) and (328, 243), we can easily estimate the size of the crack at 22.5 mm with an error of about 2.3%. The focusing array measurement provides a good means for damage detection and quantification.

When PWAS 2, 4, 5, and 6 are used to form the array (Fig. 7a), the crack lies outside the network. Imaging results are given in Fig. 8b. We have obtained clear and correct images for the 23-mm crack, even when outside the sparse array network.

Corrosion Detection with PWAS

PWAS Lamb wave SHM has also shown its capability to detect simulated corrosion (material removal) using the A0 Lamb mode in 3.229-mm-thick aluminum plates. In this study, we introduced uniform corrosion over a 50 mm × 38 mm area by machining away material. As shown in Fig. 8a, the depth was gradually increased to simulate corrosion progression. This thickness loss produced a change in the waveguide impedance and thus caused (a) scattering and reflection and (b) modification of the wave speed of Lamb waves crossing the corrosion area. The location of sensors and corrosion is illustrated in Fig. 8a.

The sensor configuration includes two general cases: on-path and off-path damage. The on-path case has damage in line with the transmitter–receiver pair, which was PWAS pair 0–4, while the off-path case has damage off the line of the transmitter–receiver pair, which was PWAS pair 1–4. More general sensor network configurations can be

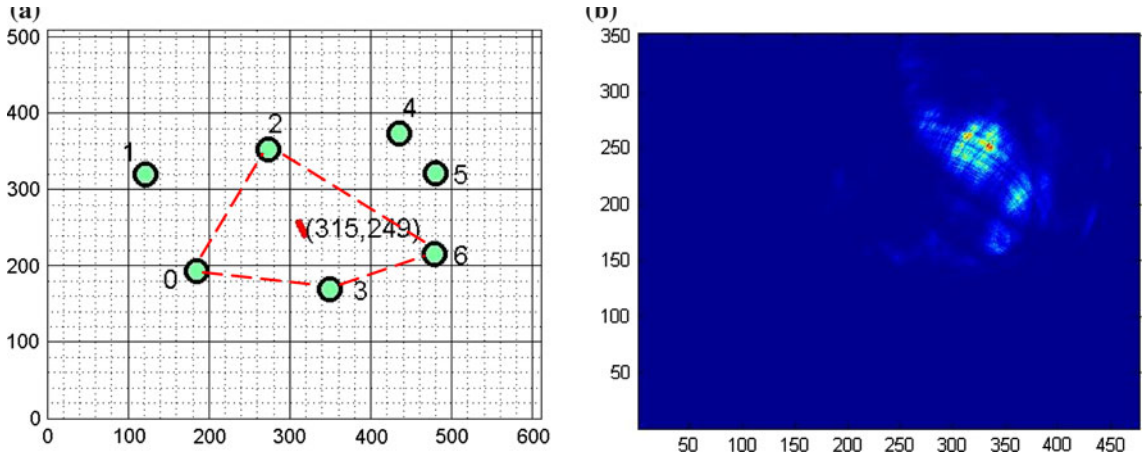

Fig. 6. Four-PWAS focusing array imaging for in-array crack detection.

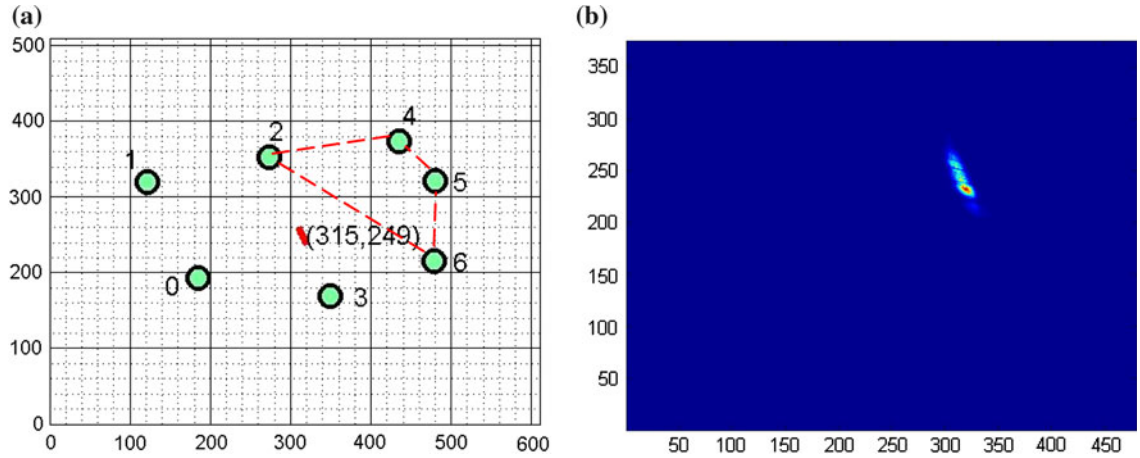

Fig. 7. Four-PWAS focusing array imaging for out-of-array crack detection.

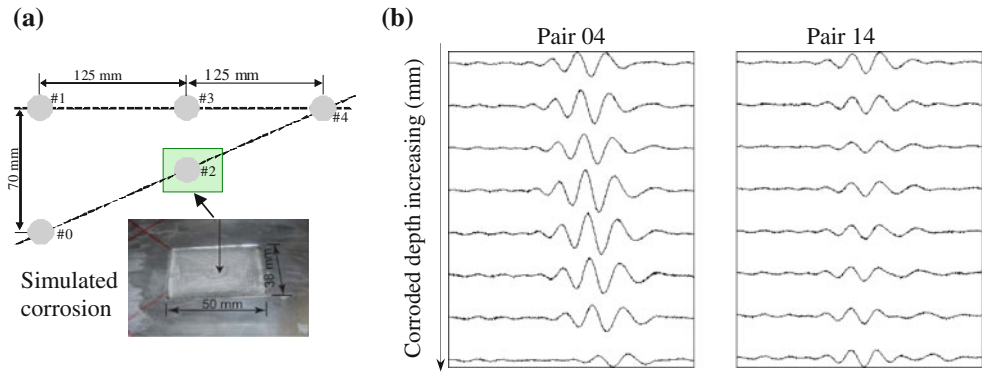

Fig. 8. Corrosion detection on an aluminum plate: (a) PWAS network configuration; (b) Lamb wave signals for pair 0–4 with significant changes and those for pair 1–4 with no discernible changes.

obtained by modifying this simplified case. The section between the on-path and off-path pairs which suffers the largest change will be considered as having corrosion. Once the path is determined, other methods such as electromechanical impedance spectroscopy (EMIS) can be used to evaluate the local EMIS changes of each sensor on the path to locate the exact position of the corrosion damage, with the PWAS acting as a thickness gage to quantify the thickness loss directly.[17] Figure 8b shows the signals received on the two paths for various corrosion depths at 57 kHz. The wave is tuned to this frequency so that the A0 mode was excited. Visual observation of these signals also implies that the A0 packets in pair 0–4 (with corrosion) have a delay in arrival time and a change (first increasing and then decreasing) in amplitude as the corrosion depth increases. In contrast, the A0 packets in pair 1–4 (no corrosion) exhibit little change in either arrival time or amplitude.

It is known that the phase of a signal is related to its delay. To evaluate the phase change during corrosion development, two approaches, one using cross spectral analysis (CPA) and one using a novel cross time–frequency analysis (CTFA), were used for data analysis to relate the signal feature to the corrosion development. CPA acquires the phase difference by using the class Fourier transform to obtain the phase value at a specific frequency (here the excitation frequency of 57 kHz) and get the phase change by taking the difference between a measurement and a reference. The resulting curves for each pair are shown in Fig. 9 (square symbols). A difference between the damaged and undamaged pair can be observed, but the resulting detection for pair 0–4 is different from the theoretical prediction of the phase change based on Lamb wave propagation theory.[18]

CTFA provides an effective tool for nonstationary signal analysis using time- and frequency-localized signal representation based on the generalized Cohen's class.[19] Based on the definition of the Wigner distribution, the cross Wigner distribution is defined in terms of the ambiguity functions

$$W_{x_1x_2}(t,\omega) = \frac{1}{2\pi}\int x_1(t+\tau/2)x_2^*(t-\tau/2)e^{-j\omega\tau}\mathrm{d}\tau. \quad (15)$$

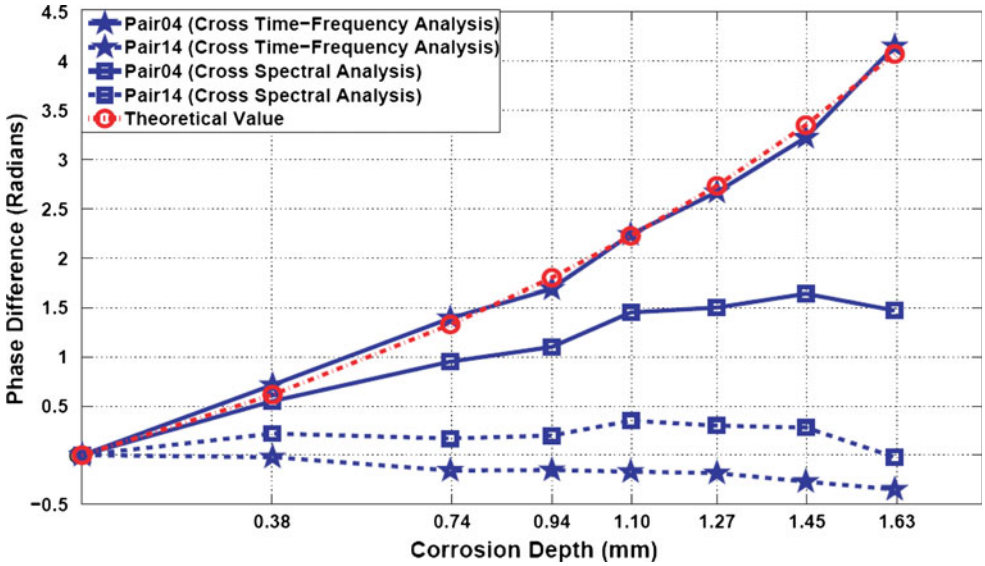

Fig. 9. Phase difference between different corrosion records and baseline for both methods.

From the cross Wigner distribution, other types of generalized cross time–frequency distribution functions, $J_{x_1,x_2}(t,\omega;\phi)$, can be obtained in terms of a kernel as

$$J_{x_1,x_2}(t,\omega;\phi)=\frac{1}{4\pi^2}\int\int W_{x_1x_2}(u,\xi)\Phi(t-u,\omega-\xi)\mathrm{d}u\mathrm{d}\xi, \tag{16}$$

where $\phi(t,\ \omega)$ is the 2D Fourier transform of the kernel $\phi(\theta,\ \tau)$. The phase analysis result using CTFA at frequency of 57 kHz and the specific A0 wave packet time duration was then obtained and is shown in Fig. 9. It can be seen that the phase differences for pair 0–4 estimated by CTFA are very close to the theoretical values, with most errors smaller than 5%, while those of pair 1–4 are around 0 radians. Thus, the phase information obtained from CTFA can determine not only the path on which the corrosion is located but also the extent of the corrosion damage.

CONCLUSIONS

This article has presented use of intelligent PWAS transducers in Lamb wave SHM. PWAS transducers can be permanently attached to structures for *in situ* health monitoring to determine the structural state of health and predict the remaining life. After reviewing the piezoelectric principles, the PWAS principle as used in Lamb wave applications (actuation and sensing) was presented. It was shown that Lamb wave mode tuning can be achieved by judicious combination of PWAS dimensions, frequency values, and Lamb wave mode characteristics; for example, the A0 and S0 Lamb modes can be separately tuned using the same PWAS installation but different frequency bands. Finally, PWAS transducers for *in situ* SHM for crack and corrosion detection were introduced. Although remarkable progress has been made in using PWAS for Lamb wave SHM, considerable work remains to be done. To increase acceptance of this emerging technology, refinement of the theoretical analysis and calibration against well-planned experiments are needed. Moreover, to deploy PWAS transducers in *in situ* SHM applications, several hurdles have still to be overcome. In particular, the operational and environmental variations of the monitored structure need to be addressed. The behavior of the bonding layer between the PWAS and the structure must be clarified as well, such that predictable and repeatable results are achieved. The durability of this bond under extended environmental exposure must also be determined. Last but not least, signal analysis methods must be developed to achieve probability of detection values at least comparable to that of conventional ultrasonic methods.

REFERENCES

1. F.P. Sun, C. Liang, and C.A. Rogers, *Proceedings of the 1994 SEM Spring Conference and Exhibits*, June 6–8, 1994.
2. Z. Chaudhry, T. Joseph, F.P. Sun, and C.A. Rogers, *Proceedings of the SPIE North American Conference on Smart Structures and Materials*, Feb. 26–March 3, 1995.
3. X. Lin and F.G. Yuan, *J. Smart Mater. Struct.* 10, 907 (2001).
4. J.B. Ihn and F.K. Chang, *Proceedings of SPIE, Smart Nondestructive Evaluation for Health Monitoring of Structural and Biological Systems*, Vol. 4702, Tribikram Kundu, June 2002, pp. 29–40.
5. K. Diamanti, C. Soutis, and J.M. Hodgkinson, *Composites A* 38, 1121 (2007).
6. APC International, *Piezoelectric Ceramics: Principles and Applications* (Ashland: APC Products Inc., 2002).
7. V. Giurgiutiu and S.E. Lyshevski, *Micro Mechatronics: Modeling, Analysis, and Design with MATLAB* (Boca Raton: CRC Press, 2004), ISBN 084931593X.
8. D.J. Leo, *Engineering Analysis of Smart Material Systems* (New York: Wiley, 2008).

9. J.L. Rose, *Ultrasonic Waves in Solid Media* (Cambridge: Cambridge University Press, 1999).
10. H. Lamb, *Proceedings of the Royal Society London A* (1917), pp. 114–128.
11. I.A. Viktorov, *Rayleigh and Lamb Waves—Physical Theory and Applications* (New York: Plenum, 1967).
12. J.D. Achenbach, *Wave Propagation in Elastic Solids* (Amsterdam: North-Holland, 1984).
13. V. Giurgiutiu, *Structural Health Monitoring with Piezoelectric Wafer Active Sensors* (Amsterdam: Academic, 2008), ISBN 9780120887606, 747 pp.
14. A. Raghavan and C.E.S. Cesnik, *Proc. SPIE* 5391, 419 (2004).
15. L. Yu and V. Giurgiutiu, *J. Mech. Mater. Struct.* 2, 459 (2007).
16. C.H. Wang, J.T. Rose, and F.K. Chang, *Smart Mater. Struct.* 13, 415 (2004).
17. L. Yu, V. Giurgiutiu, and P.J. Pollock, *Proc. SPIE* 6932, 91 (2008).
18. L. Yu, V. Giurgiutiu, J. Wang, and Y.-J. Shin, *Struct. Health Monit. Int. J.* 11, 83 (2012).
19. L. Cohen, *Proc. IEEE* 77, 941 (1989).